Geomechanics and Engineering, *Vol. 28, No. 2 (2022) 107-116*
https://doi.org/10.12989/gae.2022.28.2.107

A hysteresis model for soil-water characteristic curve based on dynamic contact angle theory

Yan Liu*[1,2] and Xu Li[1,2a]

[1]*Key Laboratory of Urban Underground Engineering of Ministry of Education, Beijing Jiaotong University, Beijing 100044, China*
[2]*School of Civil Engineering, Beijing Jiaotong University, Beijing 100044, China*

(Received October 30, 2020, Revised December 10, 2021, Accepted December 17, 2021)

Abstract. The steady state of unsaturated soil takes a long time to achieve. The soil seepage behaviours and hydraulic properties depend highly on the wetting/drying rate. It is observed that the soil-water characteristic curve (SWCC) is dependent on the wetting/drying rate, which is known as the dynamic effect. The dynamic effect apparently influences the scanning curves and will substantially affect the seepage behavior. However, the previous models commonly ignore the dynamic effect and cannot quantitatively describe the hysteresis scanning loops under dynamic conditions. In this study, a dynamic hysteresis model for SWCC is proposed considering the dynamic change of contact angle and the moving of the contact line. The drying contact angle under dynamic condition is smaller than that under static condition, while the wetting contact angle under dynamic condition is larger than that under static condition. The dynamic contact angle is expressed as a function of the saturation rate according to the Laplace equation. The model is given by a differential equation, in which the slope of the scanning curve is related to the slope of the boundary curve by means of contact angle. Empirical models can simulate the boundary curves. Given the two boundary curves, the scanning curve can be well predicted. In this model, only two parameters are introduced to describe the dynamic effect. They can be easily obtained from the experiment, which facilitates the calibration of the model. The proposed model is verified by the experimental data recorded in the literature and is proved to be more convenient and effective.

Keywords: contact angle; hysteresis; rate dependent; soil-water characteristic curve; unsaturated soil

1. Introduction

No matter rainfall infiltration or evaporation, unsaturated soil is in an unsteady state. It can even be said that in most cases, unsaturated soil, especially the top soil, is in a dynamic wetting/drying process. Traditional unsaturated soil mechanics only considers the static hydraulic characteristics of unsaturated soil, which cannot reflect the actual situation and have great differences with the actual state of soil. The dynamic effect of hydraulic characteristics of unsaturated soil should be considered. A dynamic model of hydraulic properties can help to improve the accuracy of seepage calculation of unsaturated soil.

The soil-water characteristic curve (SWCC) plays a key role to describe the dynamic process. It is defined as the relationship between the degree of saturation and suction for the soil. It is well recognized that this relationship is not unique and may exhibit hysteretic behaviour. There are typically two boundary curves, and an infinite number of scanning curves may exist between them. In many practical problems, the soil-water usually undergoes the scanning curve path rather than the boundary curve. In the early stage, numerous empirical SWCC equations were proposed (e.g., Brooks and Corey 1994, Van Genuchten 1980, Fredlund and Xing 1994). Most of these models could well predict the boundary curves, but they were incapable of predicting the scanning hysteresis loops. During the past decades, a variety of models have been proposed to predict the scanning curves, among which the linear relationship is the simplest one and has been widely introduced in constitutive models of unsaturated soils (Wheeler *et al*. 2003). Since the accuracy of the linear model was not satisfactory, some nonlinear models were proposed. Several studies (Jaynes 1984, Viaene *et al*. 1994, Pham *et al*. 2005) reviewed the nonlinear models and compared the predictions of the various hysteresis models. Most of these models required at least two boundary curves to delimit the region of admissible soil states in the space of degree of saturation and suction. Different theories were then used to predict the scanning curves between the boundaries such as the domain models (Mualem 1974), boundary surface plasticity (Li 2005, Wei and Dewoolkar 2006), pore throat hysteresis (Chen *et al*. 2020a), and contact angle hysteresis (Zhou 2013, Rafraf *et al*. 2016, Azizi *et al*. 2017). Moreover, models considering the effects of void ratio, pore size distribution, pore expansion and contraction, or stress state were developed (Zhou *et al*. 2012, Hu *et al*. 2013, Zhou and Ng 2014, Gallipoli *et al*. 2015, Otalvaro *et al*. 2016, Gao and Sun 2017, Chen *et al*. 2019, Niu *et al.* 2020).

Though the previous models gave satisfactory predictions of hysteretic behaviour, they were mostly established on the equilibrium state or based on the equilibrium test data. Noted, the water in soil does not

*Corresponding author, Associate Professor
E-mail: yanl@bjtu.edu.cn
[a]Professor
E-mail: cexuli2012@163.com

ISSN: 2005-307X (Print), 2092-6219 (Online)

necessarily flow under the equilibrium or static condition, particularly when the degree of saturation changes fast with time. Soil strength may be influenced by different water infiltration rate (Rahardjo *et al*. 2009, Rasool and Kuwano 2020). Various experimental and theoretical studies suggested that there was a discrepancy between the SWCC estimated under static and transient conditions (Topp *et al*. 1967, Smiles *et al*. 1971, O'Carroll *et al*. 2005, Camps-Roach *et al*. 2010, Sakaki *et al*. 2010, Das and Mirzaei, 2013). This phenomenon was known as the dynamic effect. Hassanizadeh *et al*. (2002) and Diamantopoulos and Durner (2012) gave comprehensive reviews of experimental observations and physical reasons about this phenomenon. Experiments indicated that the dynamic capillary pressure was larger than static capillary pressure in drying and smaller in wetting. Modelling approaches for dynamic nonequilibrium effects could be classified into two catalogues: pore-scale network models and continuum-scale models. Hassanizadeh and Gray (1993) derived a constitutive relationship for capillary pressure based on a thermodynamic framework for multiphase porous media consisting of balance laws for phases and interfaces as well as the second law of thermodynamics. These studies proposed that the difference between the nonwetting and wetting phase fluid pressures was a function of the capillary pressure under static conditions as well as the saturation rate.

$$p_c^d = p_c^e - \tau \frac{\partial S_r}{\partial t} \tag{1}$$

where, p_c^d=p_g-p_l is the nonequilibrium fluids pressure difference between air pressure p_g [kPa] and water pressure p_l [kPa]; p_c^e[kPa] is equilibrium capillary pressure; S_r is the degree of saturation; t represents time ; τ [kPa·s] is the dynamic coefficient which is a measure of the rate of change in saturation. Empirical formulae of the coefficient τ [kPa·s] have been presented in the literature. It is found to be hysteretic, and can be described by a function of saturation and matric suction both. The static and dynamic capillary pressures are only equivalent at equilibrium ($\partial S_r/\partial t$=0).

With the help of Eq. (1), the dynamic SWCC curve can be expressed. However, mainly the primary hydraulic paths, especially for the drying cases, have been studied so far. Limited experimental studies have been performed on dynamic soil-water retention behaviour during different cycles of scanning drying and wetting. Until recently, some experiments have been conducted on dynamic scanning curves (Zhuang *et al*. 2017, Milatz *et al*. 2018). Nevertheless, the theoretical models which can quantitatively describe the scanning hysteresis loops under dynamic conditions haven't been proposed yet.

In this paper, we present a dynamic hysteresis SWCC equation in the incremental form based on the dynamic contact angle theory. The contact angle approach proposed by Zhou (2013) is integrated into the dynamic model. Traditional empirical SWCC models can be used as the static boundary branch, and a dynamic boundary is derived from Eq. (1). The relationship between the slope of the scanning curve and the boundary curve is obtained based on dynamic contact angle theory. Some test results documented in the literature are used to validate our proposed SWCC equation.

2. Dynamic contact angle hysteresis theory

Studies indicated that SWCC shows hysteretic effect and dynamic effect. Various reasons have been used to explain these two effects. The major mechanisms of hysteretic effect may be attributed to many factors, including ink-bottle effect due to non-uniformity of pores, snap off effect due to the entrapment air or water, soil deformation and contact angle hysteresis (Albers 2014). Alves *et al.* (2020) pointed out hysteresis phenomena may be partially considered through the use of adequate contact angles. Liu *et al.* (2013) indicated that contact angle could have a major effect on the SWCCs. The major potential mechanisms of dynamic effect suggested in the literature are air entrapment, water entrapment, air-water interface reconfiguration, dynamic contact angle and heterogeneity on both the microscopic and macroscopic scale. Camps-Roach *et al*. (2010) proposed that pore water and air entrapment did not likely contribute to observing dynamic capillary pressure effects, and dependency of contact angle might be considered as a major and more plausible phenomenon. Referring to the above mechanisms, we can find that the contact angle theory can be used to explain both the hysteretic and dynamic phenomenon. Therefore, the contact angle theory is used as a theorical basis for our proposed model.

The contact angle is the tangent of the drop profile at the three-phase contact point where the liquid-gas interface meets the solid-liquid interface. Good (1992) presented a general review of contact angle. It is not constant but varies between the maximum contact angle and minimum contact angle, which are termed as the advancing contact angle, θ_A, and the receding contact angle, θ_R, respectively. The difference between the advancing and the receding contact angle is the so-called contact angle hysteresis (Eral *et al.* 2013). When a three-phase contact line moves along a solid surface, the contact angle no longer corresponds to the static equilibrium angle. It is observed that the dynamic advancing contact angle increases with the increase of velocity, while the dynamic receding contact angle decreases with the increase of velocity (Friedman 1999). Under dynamic conditions, the utility of static contact angles to characterize wetting and drying is limited.

The mechanism of contact angle hysteresis can be discussed on the pore scale shown in Fig. 1. Initially the contact angle is θ at the meniscus line 1 in Fig. 1. If the capillary pressure decreases due to externally disturbance, the position of the water meniscus initially remains unchanged, and the contact angle increases (Fig. 1(a)). Once the contact angle reaches the advancing contact angle θ_A^e (line 2 in Fig. 1(a)), it remains constant, and further decreasing capillary pressure will cause the water meniscus to move to the right. The two processes are known as pinning and slipping. However, the advancing contact angle

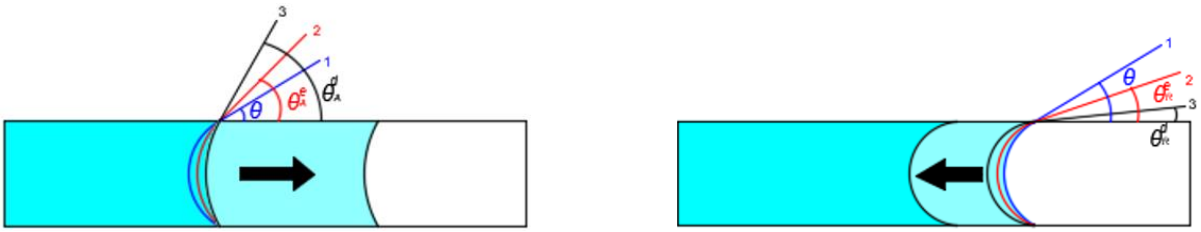

(a) Advancing contact angle during wetting path (b) Receding contact angle during drying path

Fig. 1 Schematic model of dynamic contact angle

is not fixed, but varies with the flow rate (Friedman 1999). In a transient flow, the advancing contact angle may become θ_A^d (line 3 in Fig. 1(a)). In contrary, if the capillary pressure is increased, the contact angle will decrease to the receding contact angle θ_R^e under static condition (line 2 in Fig. 1(b)) or θ_R^d (line 3 in Fig. 1(b)) under dynamic condition. Afterwards, further increase of the capillary pressure will cause the water meniscus to slip to the left.

There are various approaches to modeling the retention of liquid-gas phases in a porous medium, in most of which the pore system is considered as a bundle of cylindrical capillaries (Friedman 1999). The capillary pressure for a circular tube is described by the Young-Laplace equation

$$p_c^e = \frac{2\gamma^{lg}\cos\theta^e}{r} \tag{2}$$

where r [m]is the mean radius of the capillary tube; γ^{lg} [N/m] is the liquid/gas interfacial tension; θ is the contact angle between the air-water-solid interface. Eq. (2) is obtained at equilibrium state, and thus the contact angle is static θ^e.

Substituting Eq. (2) into Eq. (1) yields

$$p_c^d = \frac{2\gamma^{lg}}{r}\left(\cos\theta^e - \tau'\frac{\partial S_r}{\partial t}\right) \tag{3}$$

where, $\tau' > 0$ is a converted dynamic coefficient, and is expressed as

$$\tau' = \frac{r}{2\gamma^{lg}}\tau \tag{4}$$

The dynamic contact angle can then be expressed as

$$\cos\theta^d = \cos\theta^e - \tau'\frac{\partial S_r}{\partial t} \tag{5}$$

According to Eq. (5), during drying dS_r <0 results in θ^d<θ^e; while during wetting, dS_r >0 results in θ^d>θ^e. It is in accordance with the concept shown in Fig. 1. Researchers have found that the dynamic contact angle is mainly determined by the interplay between viscous and capillary forces. Two different models have been proposed in the literature to describe the dependence of dynamic contact angles on contact line velocity: hydrodynamic model and molecular-kinetic model (Eral *et al.* 2013). In these models, the contact angle is described as a function of the contact line velocity within the single pore. The saturation rate in Eq. (5) is related to the macroscopic liquid flux, which is

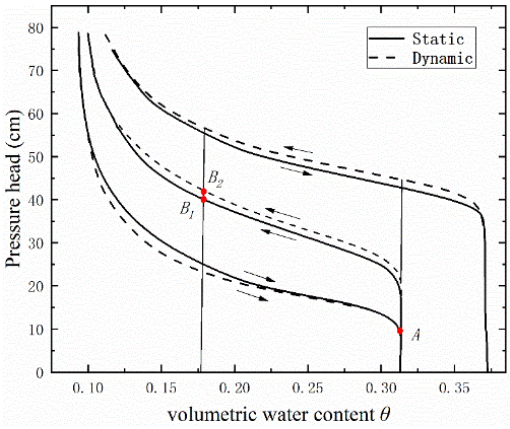

Fig. 2 Conceptual SWCC under different conditions (after Wana-etyem, 1982)

corresponded to contact line velocity on the pore scale. Thus, Eq. (5) is consistent with the previous models.

Since the maximum contact angle θ_A^d is larger than θ_A^e in wetting process and the minimum contact angle θ_R^d is smaller than θ_R^e in drying process. This phenomenon could result in a higher capillary pressure for drying process and a lower capillary pressure for wetting process under dynamic conditions compared with static conditions. Fig. 2 shows the hysteresis SWCC curve based on experiments (Wana-etyem, 1982), where the solid line represents the static condition, and the dashed line represents the dynamic condition. It is assumed that the contact angle remains a receding contact angle on the drying boundary curve and an advancing contact angle on the wetting boundary curve (Zhou 2013). Under the static condition, the contact angle decreases from θ_A^e (point A) to θ_R^e (point B_1) for the drying scanning curve. However, under the dynamic condition, for the same variation of saturation, the contact angle decreases from θ_A^d (point A) to θ_R^d (point B_2) for drying process. The variation of suction in dynamic condition is larger than that in static condition, which may have significant effect on the soil strength and deformation.

3. A dynamic hysteresis model

Although several SWCC models based on the contact angle hysteresis have been proposed (Zhou 2013, Rafraf *et al.* 2016, Azizi *et al.* 2017), the velocity-dependent dynamic contact angle effect is commonly not included. During the transient flow process the contact angle varies between θ_A^d

and θ_R^d, rather than θ_A^e and θ_R^e. Eq. (3) indicates that the capillary pressure can also be calculated by the Young-Laplace equation, but with the dynamic contact angle, θ^d, rather than with the static one. During dynamic condition, the nonequilibrium pressure is given as

$$p_c^d = \frac{2\gamma^{lg}\cos\theta^d}{r} \tag{6}$$

To predict the scanning curve, two boundary curves, which delimit the region of admissible soil states in the space of degree of saturation and suction, are required. The suction on the scanning curve is related to the suction on the boundary curve.

$$s = \frac{\cos\theta}{\cos\theta^d} p_c^d \tag{7}$$

where θ is the current contact angle. θ^d is the contact angle on the boundary curve, $\theta^d = \theta_A^d$ for wetting process and $\theta^d = \theta_R^d$ for drying process. To avoid confusion, s [kPa] hereinafter represents the nonequilibrium capillary pressure on the scanning curve, and p_c^d [kPa] hereinafter represents the nonequilibrium capillary pressure on the main drying or wetting curve.

The slope of the dynamic boundary curve is derived from Eq. (1)

$$\bar{K}^d = -\frac{\partial p_c^d}{\partial S_r} = -\frac{\partial p_c}{\partial S_r} + \frac{\partial \tau}{\partial S_r}\dot{S}_r = \bar{K} + \frac{\partial \tau}{\partial S_r}\dot{S}_r \tag{8}$$

where, $\bar{K}^d$ [kPa] represents the slope of dynamic boundary curve; $\bar{K}$ [kPa] represents the slope of static boundary curve, which can be derived from the traditional SWCC equation; $\dot{S}_r$ is the time derivative of degree of saturation.

The slope K of the scanning curve is obtained from the derivation of Eq. (7)

$$\begin{aligned} K &= -\frac{\partial s}{\partial S_r} = -\frac{\cos\theta}{\cos\theta^d}\frac{\partial p_c^d}{\partial S_r} + p_c^d \frac{\sin\theta}{\cos\theta^d}\frac{\partial \theta}{\partial S_r} \\ &= \frac{\cos\theta}{\cos\theta^d}\bar{K}^d + s\tan\theta\frac{\partial\theta}{\partial S_r} \end{aligned} \tag{9}$$

Contact angle is a function of the capillary pressure rather than saturation according to Eq. (6). Hence, Eq. (9) can be rewritten as

$$K = \frac{\cos\theta}{\cos\theta^d}\bar{K}^d - s\tan\theta\frac{\partial\theta}{\partial s}K \tag{10}$$

By solving Eq. (10), we obtain

$$K = \left(1 + s\tan\theta\frac{\partial\theta}{\partial s}\right)^{-1}\frac{\cos\theta}{\cos\theta^d}\bar{K}^d \tag{11}$$

According to the method proposed by Zhou (2013), the derivative of contact angle with respect to the capillary pressure is expressed as

$$\frac{\partial\theta}{\partial s} = -k\frac{1}{s\tan\theta} \tag{12}$$

where the parameter k is used to quantify the allocation proportion for the suction increment that further affects the hysteresis pattern of a soil.

Substituting Eq. (12) into Eq. (11) yields

$$K = \frac{1}{1-k}\frac{\cos\theta}{\cos\theta^d}\bar{K}^d \tag{13}$$

During the pinning process shown in Fig. 1, the change of water saturation is negligible. It is thus assumed that the suction varies solely due to the change of contact angle. In this case, the scanning curve is vertical initially in the S_r - p_c space shown in Fig. 2, which means the initial slope is infinite, and the initial value of k equals to 1. When the meniscus starts to move, the contact angle is thought to be constant and k decreases. Once the scanning path reaches the boundary curve, the slope K is equal to the boundary curve $\bar{K}^d$, which means the value of k is equal to 0 according to Eq. (13).

The parameter k varies between 1 and 0, and can be represented as (Zhou 2013)

$$k = \begin{cases} \left(\dfrac{\cos\theta_R^d - \cos\theta}{\cos\theta_R^d - \cos\theta_A^d}\right)^b, & dS_r < 0 \\ \left(\dfrac{\cos\theta - \cos\theta_A^d}{\cos\theta_R^d - \cos\theta_A^d}\right)^b, & dS_r > 0 \end{cases} \tag{14}$$

where the parameter b ($0 < b < 1$) controls the extent of contact angle variation of scanning curve.

Various methods have been proposed for the measurement of contact angles of soils. For example, Liu *et al*. (2016) applied of the capillary rise method to measure the contact angles of soils. For simplicity we could substitute Eq. (7) into Eq. (14). The parameter k can be calculated by

$$k = \begin{cases} \left(\dfrac{p_{cD}^d - s}{p_{cD}^d - p_{cW}^d}\right)^b, & dS_r < 0 \\ \left(\dfrac{s - p_{cW}^d}{p_{cD}^d - p_{cW}^d}\right)^b, & dS_r > 0 \end{cases} \tag{15}$$

where, p_{cD}^d [kPa] and p_{cW}^d [kPa] are the capillary pressures of dynamic drying boundary curve and wetting boundary curve, respectively; $(p_{cD}^d - p_{cW}^d)$ represents the horizontal distance between two boundary curves in Fig. 2; $(p_{cD}^d - s)$ or $(s - p_{cW}^d)$ represents the horizontal distance between the current state and the related boundary curves. Eq. (15) is similar to some existing models (Li 2005), in which the SWCC with hysteresis is defined as the distance from the current state to the boundary curve.

The suction increment is then calculated by

$$ds = -KdS_r = -\frac{1}{1-k}\frac{s}{p_c^d}\bar{K}^d dS_r \tag{16}$$

Given the static boundary curve by some empirical models, the slope of the dynamic boundary curve can be obtained by Eq. (8). The sign of dS_r is required to determine drying or wetting. The slope of the scanning

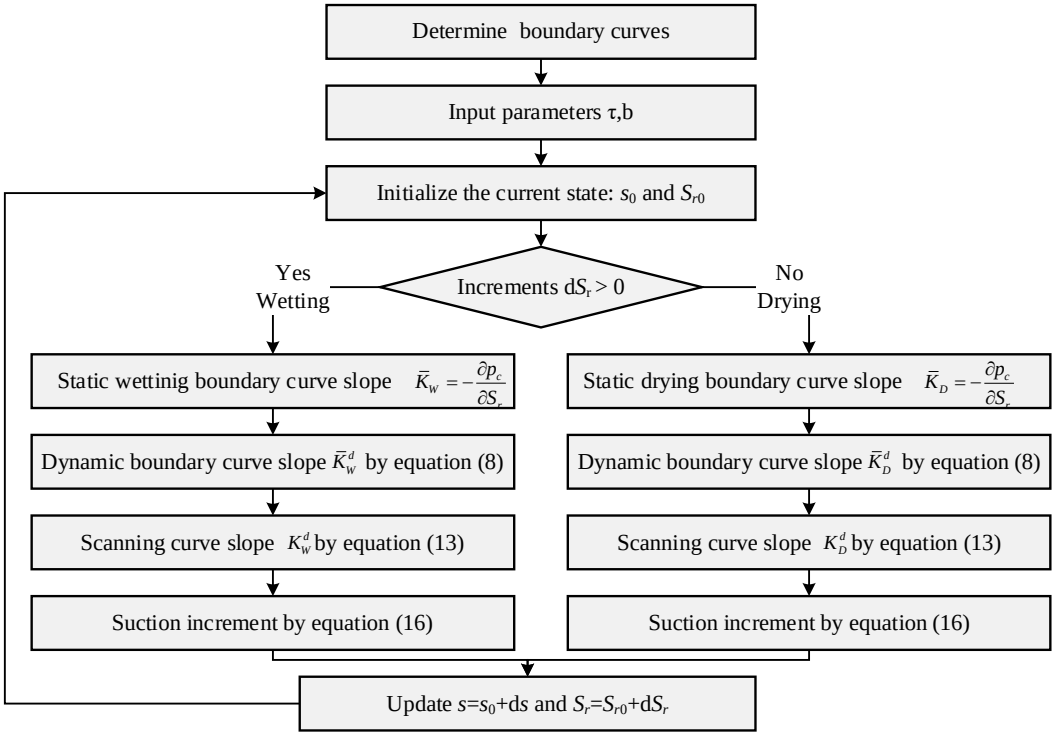

Fig. 3 Algorithm of dynamic hysteresis model

curve is then calculated by Eq. (13). The scanning curve is predicted by a differential Eq. (16). The complete algorithm for this model is shown in Fig. 3.

The previous model uses the same equation (Eq. (1)) to simulate both the boundary curve and scanning curve. The parameters of different scanning lines will be different. It is not convenient to predict scanning curves without experiment. The scanning line parameter τ itself is not easy to calibrate, especially when the saturation change rate is not constant. However, the proposed model here uses the boundary curve to predict the scanning curve. Given the boundary line and parameters τ and b, the model can predict the scanning line. The advantages of this are as follows: (1) the proposed contact angle model is not an empirical function but has a strictly theoretical basis. (2) parameter b is used to predict the scanning curve. It can be calibrated by at least one scanning curve. And then we can use it to predict any other scanning curve.

4. Model validation

Our model is used to predict the experimental data to illustrate the capabilities of the model. The dynamic test data in the literature are utilized to verify our proposed model in this section. The data on the dynamic scanning curves are limited due to time-consuming measurement. We find only two sets of data (Zhuang *et al.* 2017, Milatz *et al.* 2018) are suitable for further analysis based on our comprehensive review. These data are used to validate our model. The validation of the static model is presented by Zhou (2013). We will focus on the dynamic hysteresis behaviour in this research.

4.1 Model calibration

Firstly, two boundary curves are required. They can be obtained from classical SWCC models such as VG model.

$$p_c^e = a\left[S_e^{n/(1-n)} - 1\right]^{1/n} \tag{17}$$

where, a and n are model parameters, $S_e = (S_r - S_{ir})/(1 - S_a - S_{ir})$ is the effective saturation, S_{ir} and S_a are the irreducible water saturation and the residual air saturation respectively.

Substituting Eq. (17) into Eq. (1), the boundary curve of dynamic SWCC is obtained

$$p_c^d = a\left[S_e^{n/(1-n)} - 1\right]^{1/n} - \tau \dot{S}_r \tag{18}$$

The slope of static boundary curve is given by

$$\bar{K} = -\frac{\partial p_c}{\partial S_r} = \frac{1}{n-1}\frac{a}{S_r - S_{ir}}\left[S_e^{n/(1-n)} - 1\right]^{(1+1/n)} \tag{19}$$

Substituting Eq. (19) into Eq. (8), the slope of dynamic boundary curve is obtained.

$$\bar{K}^d = \frac{1}{n-1}\frac{a}{S_r - S_{ir}}\left[S_e^{n/(1-n)} - 1\right]^{(1+1/n)} + \frac{\partial \tau}{\partial S_r}\dot{S}_r \tag{20}$$

Following the algorithm in Fig.3, the scanning curve can be predicted. The above algorithm can be realized by MATLAB software.

There are two parameters τ and b in our model in addition to the SWCC parameters a and n. If τ=0, our model degrades into the static hysteresis model. The calibration method of parameters a, n and b is the same as traditional SWCC (Zhou 2013). The main drying curve is employed to

Table 1 Model Parameters

Experiment source	Residual air saturation S_a	irreducible water saturation S_{ir}	Drying		Wetting		b
			a(cm)	n	a(cm)	n	
Zhuang *et al*. (2017)	0.14	0.21	35.5	9.5	22.2	10.2	0.18
Milatz *et al*. (2018)	0	0.18	5.5	9.2	2.5*	9.2*	0.55

*These parameters are assumed according to Likos and Lu (2014) due to lack of experiment data

calibrate two van Genuchten's fitting parameters (a and n). A scanning wetting branch is used to calibrate the hysteresis curvature parameter b. The parameter τ can be calculated by Eq. (1). To calibrate parameter τ, information is needed on the difference between p_c^d andp_c^e, and on the time rate of change of saturation or water content. However, the parameter τ is most probably not constant and may vary with saturation. The value τ in the literature varies over a wide range. Hassanizadeh *et al*. (2002) calculated the approximate value of τ, ranging from 3×10^4 to 5×10^7 Pa·s. In the following predictions, the parameter τ is obtained from references which are calibrated from test data.

4.2 Predictions for dynamic drying experiments

Zhuang *et al*. (2017) performed a series of dynamic drying experiments on a small-volume unsaturated sandy soil. The relationships between capillary pressure and saturation were first measured under quasi-static conditions. Afterwards, the primary, main, and scanning drying experiments were carried out to investigate the capillarity effect during dynamic drying. The experiment data obtained during the quasi-static condition and dynamic condition are shown in Fig. 4. The primary drying curve and main wetting curve are chosen as the boundary curves. The static SWCC parameters a and n can be derived by static boundary data, and the parameter b is calibrated by static scanning curve. The results are shown in Table 1.

The rate of change in saturation with time $\dot{S}_r$, is calculated using a backward difference approximation. The absolute values of $\dot{S}_r$ in dynamic drying experiments increase dramatically to reach a maximum value, and then gradually approach zero. The maximum absolute value is found to be 0.05 s^{-1} during main drying. It is used as the upper boundary of all curves. The parameter τ is required to calculate the dynamic boundary curves. A log-linear function between τ and S_r is given by Zhuang *et al*. (2017)

$$\lg\tau = 2.0 - 0.094\left(S_r - S_{r0}\right) \tag{21}$$

where, lg represent log10; S_{r0} is the threshold value. S_{r0}=0.85 for primary drying curve, S_{r0}=0.73 for main drying curve, and S_{r0}=0.53 for scanning curve. Since the dynamic wetting data are not available, the dynamic wetting curve is calculated based on the static wetting curve by Eq. (18), in which S_{r0}=0.73 for main drying curve is used.

The predictions of our model are shown in Fig. 4, where the solid and the dashed lines represent the static and the dynamic curves, respectively. It can be found that the dynamic effect obviously influences the scanning behaviour. The results of our model show good agreement

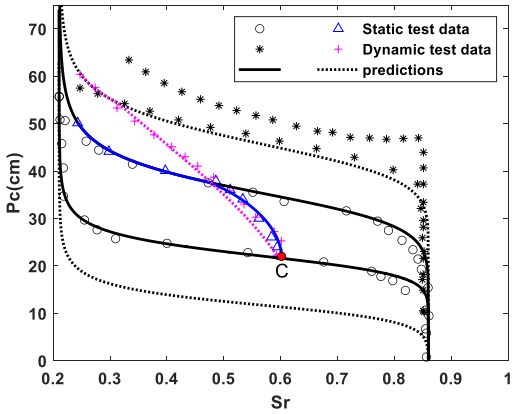

Fig. 4 Predictions for dynamic drying test

with the test data. It is clear that at a given saturation (from 0.6 to about 0.25), the air-water pressure difference for dynamic scanning drying initially coincides with the static capillary pressure at point C, and then it becomes larger. Normally, it would be expected that the scanning curve is inside the boundary curves. If we used the static hysteresis model here, the red dashed line beyond the static boundary curve could not be described. In our model, the drying boundary curve shifts upward due to dynamic effect. Therefore, the scanning curve (red line) remains inside the boundaries, and can be well described.

4.3 Predictions for dynamic hysteresis loops

Milatz *et al*. (2018) conducted a series of experiment to examine the influence of the rate of change of saturation on the transient water retention curves of granular soils with a low suction range. Two different grains of sand were used, a medium coarse-grained sand and a fine-grained sand. The rate effect on the fine-grained sand is more significant in comparison to that of the coarse-grained sand. Thus, the results of fine-grained sand are used in this paper.

We use the equilibrium test data points shown in Fig. 5 to calibrate the parameters a, n and b. The parameter values are shown in Table 1. Since the wetting data are not given, we assume the value for wetting parameters a_W and n_W according to Likos and Lu (2014). Likos and Lu (2014) studied the uncertainty of a and n for 25 diverse soils and suggested the following relation a_W=*0.45*a_D, n_W=n_D.The dynamic parameter τ (kPa·s) increases with the decrease of S_r, and the relationship is given by Milatz *et al*. (2018)

$$\tau = 5281.2 - 379.5\times S_r \tag{22}$$

Eq. (22) is evaluated by the drying data, and are used

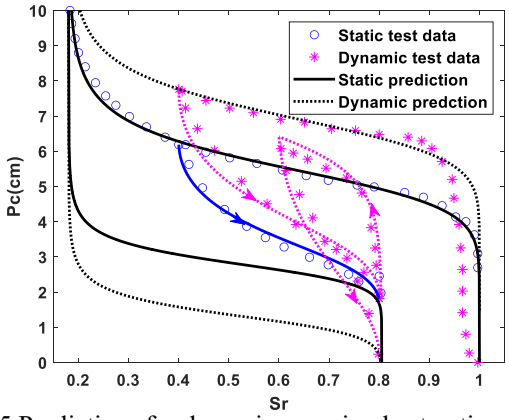

Fig. 5 Predictions for dynamic scanning hysteretic curves

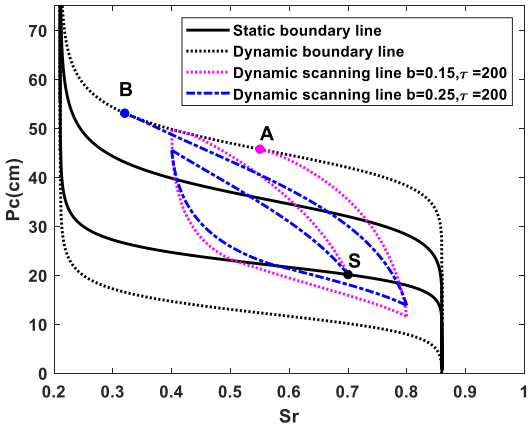

Fig. 6 Influences of parameter b

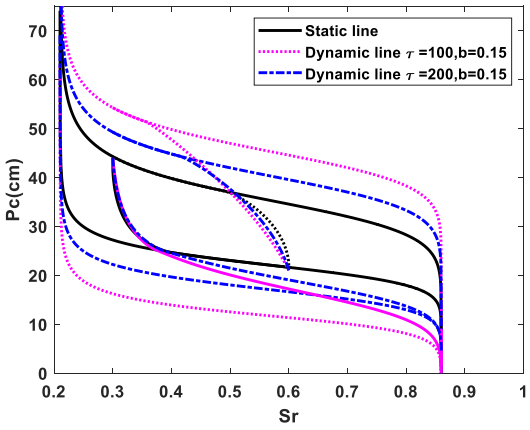

Fig. 7 Influences of parameter τ

for both drying and wetting curve due to lack of wetting data. The initial conditions with void ratio e_0 = 0.8 and S_r = 1 and test results with flow rate q=5 mm^3/s are shown in Fig. 5. The corresponding rate of saturation is 2.9×10^{-4} s^{-1}, and the variation of the degree of saturation is 1-0.4-0.8-0.6-0.8.

Our predictions are compared with the experiment results (Fig. 5). The solid line represents the equilibrium results, and the dashed line represents the dynamic results. A difference between the first wetting path and consecutive cyclic wetting paths can be noticed. The dynamic hysteresis loop shrifts upward, which is beyond the equilibrium boundaries. Since the reduction of the sand void ratio (from 0.80 to 0.79) is negligible, the drift is caused by the dynamic effects rather than the soil deformation. It is shown that the predictions are in good agreement with the dynamic hysteresis loops. The dynamic effects can be well described by our proposed model.

5. Sensitivity analysis

To show the model performance and sensitivity of model parameters, the test results given by Zhuang *et al* (2017) is used as a reference in this section. The van Genuchten's fitting parameters are given in Table 1. The influences of parameters b and τ on model features are shown in this section.

5.1 Influence of parameter b

A given drying/wetting path is shown in Fig. 6. The degree of saturation starts from 0.7 (point S), first drying to 0.4, then wetting to 0.8, followed by a drying path to the boundary curve. The model has the same parameters except parameter b. Parameter b controls the secant slope of the non-linear scanning curves. Increasing the value of parameter b inclines the non-linear scanning curve accordingly. For the same variation of the degree of saturation, the change of suction is large with a small value of b.

5.2 Influence of parameter τ

The parameter τ may be interpreted as a measure of the speed with which a change in saturation takes place. Fig. 7 shows the influence of parameter τ on the model. In this case, the model has the same parameters except parameter τ. Two series scanning lines for drying and wetting are given. They start from the same points on the static boundary line but ended in different positions. The variation of suction is big with a big value of τ.

The parameter τ represents the dynamic effect of the models. It is most probably not constant and may varied with saturation. To further explore the influence of the variation of this parameter on the model, the relative difference of suction is defined.

$$\Delta s = \frac{s(\tau) - s(\tau_0)}{s(\tau_0)} \times 100\% \tag{23}$$

where Δs is the relative difference between suction estimated by varied τ and constant τ_0, $s(\tau_0)$ means the suction is calculated by a constant $\tau_0 = 200kPa \cdot s$, $s(\tau)$ means the suction is calculated by parameter τ given by Eq. (21).

Fig. 8 shows the relative difference of suction for different drainage conditions. The drying lines start from the static boundary line with S_r=0.6 and the wetting lines start from the static boundary line at S_r=0.3. The values Δs at these start points equal to 0. And then the difference become bigger. It can be found that the dynamic suction

calculated by τ is bigger than τ_0. However, the difference is very small ($\Delta s<2\%$).

5.3 Influence of time rate of degree of saturation

The time rate of degree of saturation is set to be constant in the above predictions. However, it is not constant due to the heterogeneity of soil. It is influenced by not only the permeability characteristics of water (the permeability coefficient is varied during drying/wetting path), but also the deformation of soil. The time rate of saturation was difficult to measure and was calculated using a backward difference approximation. In the above simulation, an average value of $\dot{S}_r$ is assumed. The errors caused by variation of saturation rate are then reflected in parameter τ. In this section the influence of the time rate of degree of saturation is discussed.

It is hard to give the expression of $\dot{S}_r$. An empirical function of test data in Fig. 9 is used

$$S_r = 0.86 - 0.08 \ln t \tag{24}$$

As shown in Fig. 9, the function could well predict the saturation variation. The time derivative of saturation can be calculated b

$$\dot{S}_r = -0.08 \exp\left[12.5(S_r - 0.86)\right] \tag{25}$$

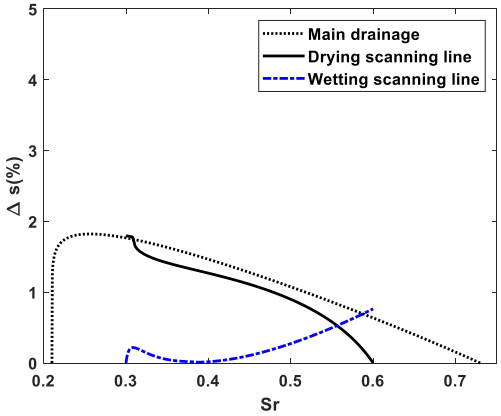

Fig. 8 relative difference of suction induced by parameter τ

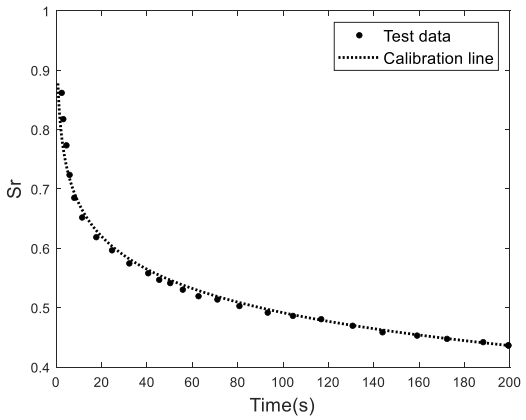

Fig. 9 relationship between the degree of saturation and time of main drying curve (after Zhuang *et al*. 2017)

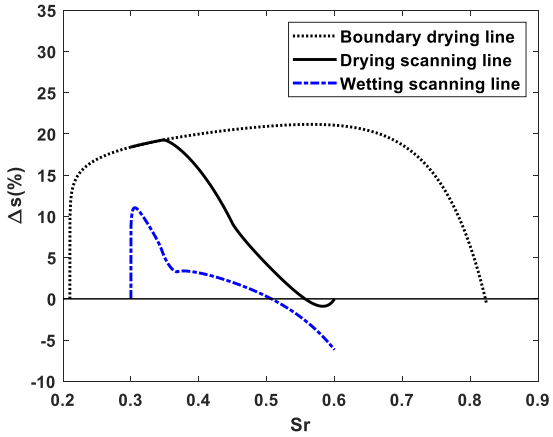

Fig. 10 relative difference of suction induced by saturation rate $\dot{S}_r$

Substituting Eq. (25) into Eq. (8), and assuming τ is constant, the slope of dynamic boundary curve is obtained.

$$\bar{K}^d = \frac{1}{n-1}\frac{a}{S_r - S_{ir}}\left[S_e^{n/(1-n)} - 1\right]^{(1+1/n)} + \tau\frac{\partial \dot{S}_r}{\partial S_r} \tag{26}$$

Eq. (26) is then used to predict the scanning line.

The relative difference of suction in Fig. 10 is calculated by

$$\Delta s = \frac{s(\dot{S}_r) - s(\dot{S}_{r0})}{s(\dot{S}_{r0})} \times 100\% \tag{27}$$

where, $s(\dot{S}_{r0})$ means the suction is calculated by a constant $\dot{S}_{r0}$=-0.05s^{-1}; $s(\dot{S}_r)$means the suction is calculated with Eq. (25). It is noted that the test data is not given during wetting path, we assumed that there is no difference between the wetting boundary line.

The difference of suction is shown in Fig. 10. The drying lines start from the static boundary line with S_r=0.6 and the wetting lines start from the static boundary line at S_r=0.3. The values Δs at these start points equal to 0. For a drying path, the suction difference is small and negative. The value become positive and bigger with the S_r decrease. For a wetting path, the suction difference is positive, and become negative in the end. The maximum difference is small then 22%, which is bigger than Fig. 8. That means the influence of saturation rate may be larger than parameter τ.

6. Conclusions

This paper presents a dynamic hysteresis SWCC model based on the dynamic contact angle theory. It is well known that the SWCC relationship depends on both the history and rate of change of saturation. The dependence on history is known as hysteresis and can be accounted for by contact angle hysteresis. The dependence on the rate is known as the dynamic effect and can be considered by the dynamic contact angle theory. Thus, the dynamic contact angle hysteresis theory can be used to explain the dynamic hysteresis behaviour.

Our model is defined by a differential equation, in which the parameter k, described by a function of the dynamic contact angles, is used to control the relationship between the slope of scanning curves and boundary curves. Given the two boundary curves by experimental results, the dynamic scanning curve can be simulated. There are only two parameters b and τ in our model in addition to the SWCC parameters. Our proposed model against previous sandy soil test data in the literature is given, demonstrating that the model is easy to apply and accurate.

A dynamic model of hydraulic properties can help to improve the accuracy of seepage calculation of unsaturated soil. Further development of the model can be made on experiments, models, and applications. More tests are needed to explain and verify the model. Additionally, experiments that consider soil deformation and other effects are also needed to develop the model. The accurate description of the SWCC is of great importance due to its essential for soil behavior. The proposed model can be used to describe the deformation, strength, and seepage behavior in soils

Acknowledgements

The research described in this paper was financially supported by the Fundamental Research Funds for the Central Universities (2019JBM086).

References

Albers, B. (2014), "Modeling the hysteretic behavior of the capillary pressure in partially saturated porous media: A review", *Acta Mech*., **225**(8), 2163-2189. https://doi.org/10.1007/s00707-014-1122-4.

Alves, R.D., Gitirana Jr., G. and Vanapalli, S.K. (2020), "Advances in the modeling of the soil–water characteristic curve using pore-scale analysis", *Comput. Geotech.*, **127**(4), 103766. https://doi.org/10.1016/j.compgeo.2020.103766.

Azizi, A., Jommi, C. and Musso, G. (2017). "A water retention model accounting for the hysteresis induced by hydraulic and mechanical wetting-drying cycles", *Comput. Geotech*., **87**(1), 86-98. https://doi.org/10.1016/j.compgeo.2017.02.003.

Camps-Roach, G., O'Carroll, D.M., Newson, T.A., Sakaki, T. and Illangasekare, T.H. (2010), "Experimental investigation of dynamic effects in capillary pressure: Grain size dependency and upscaling", *Water Resour. Res*., **46**(8), W08544. https://doi.org/10.1029/2009WR008881.

Chen, H., Chen, K., Yang, M. and Xu, P. (2020a), "A fractal capillary model for multiphase flow in porous media with hysteresis effect", *Int. J. Multip. Fl.*, **125**(1), 103208. https://doi.org/10.1016/j.ijmultiphaseflow.2020.103208.

Chen, H., Chen, K. and Yang, M. (2020b), "A new hysteresis model of the water retention curve based on pore expansion and contraction", *Comput. Geotech.*, **121**(12), 103482. https://doi.org/10.1016/j.compgeo.2020.103482.

Chen, R., Liu, P., Liu, X., Wang, P. and Kang, X. (2019), "Pore-scale model for estimating the bimodal soil–water characteristic curve and hydraulic conductivity of compacted soils with different initial densities", *Eng. Geol*., **260**, 105199. https://doi.org/10.1016/j.enggeo.2019.105199.

Das, D.B. and Mirzaei, M. (2013), "Experimental measurement of dynamic effect in capillary pressure relationship for two-phase flow in weakly layered porous media", *Aiche J*., **59**(5), 1723-1734. http://doi.org/10.1002/aic.13925.

Diamantopoulos, E. and Durner, W. (2012), "Dynamic nonequilibrium of water flow in porous media: A review", *Vadose Zone J*., **11**(3), vzj2011.0197. http://doi.org/10.2136/vzj2011.0197.

Eral, H.B., Mannetje, D.T. and Oh, J.M. (2013), "Contact angle hysteresis: a review of fundamentals and applications", *Colloid Polym. Sci*., **291**(2), 247-260. http://doi.org/10.1007/s00396-012-2796-6.

Friedman, S.P. (1999), "Dynamic contact angle explanation of flow rate-dependent saturation-pressure relationships during transient liquid flow in unsaturated porous media", *J. Adhes. Sci. Technol*., **13**(12), 1495-1518. http://doi.org/10.1163/156856199X00613.

Gallipoli, D., Bruno, A.W., D'Onza, F. and Mancuso, C. (2015), "A bounding surface hysteretic water retention model for deformable soils", *Géotechnique*, **65**(10), 793-804. http://doi.org/10.1680/jgeot.14.P.118.

Gao, Y. and Sun, D. (2017), "Soil-water retention behavior of compacted soil with different densities over a wide suction range and its prediction", *Comput. Geotech*., **91**(1), 17-26. https://doi.org/10.1016/j.compgeo.2017.06.016.

Good, R.J. (1992), "Contact angle, wetting, and adhesion: a critical review", *J. Adhes. Sci. Technol.*, **6**(12), 1269-1302. https://doi.org/10.1163/156856192X00629.

Hassanizadeh, S.M. and Gray, W.G. (1993), "Thermodynamic basis of capillary pressure in porous media", *Water Resour. Res*., **29**(10), 3389-3405. http://doi.org/10.1029/93WR01495.

Hassanizadeh, S.M., Celia, M.A. and Dahle, H.K. (2002), "Dynamic effect in the capillary pressure–saturation relationship and its impacts on unsaturated flow", *Vadose Zone J*., **1**(1), 38-57. http://doi.org/10.2136/vzj2002.3800.

Hu, R., Chen, Y.F., Liu, H.H. and Zhou, C.B. (2013), "A water retention curve and unsaturated hydraulic conductivity model for deformable soils: Consideration of the change in pore-size distribution", *Géotechnique*, **63**(16), 1389-1405. https://doi.org/10.1680/geot.12.P.182

Jaynes, D.B. (1984), "Comparison of soil-water hysteresis models", *J. Hydrol.*, **75**(1), 287-299. https://doi.org/10.1016/0022-1694(84)90054-4.

Li, X.S. (2005), "Modelling of hysteresis response for arbitrary wetting/drying paths", *Comput. Geotech.*, **32**(2), 133-137. https://doi.org/10.1016/j.compgeo.2004.12.002.

Likos, W.J., Lu, N. and Godt, J.W. (2014), "Hysteresis and uncertainty in soil water-retention curve parameters", *J. Geotech. Geoenviron.*, **140**(4), 04013050. https://doi.org/10.1061/(ASCE)GT.1943-5606.0001071.

Liu, Z., Yu, X. and Wan, L. (2013), "Influence of contact angle on soil–water characteristic curve with modified capillary rise method", *Transport. Res. Rec.*, **2349**(1), 32-40. https://doi.org/10.3141/2349-05.

Liu, Z., Yu, X. and Wan, L. (2016), "Capillary rise method for the measurement of the contact angle of soils", *Acta Geotech.*, **11**(1), 21–35. https://doi.org/10.1007/s11440-014-0352-x.

Milatz, M., Törzs, T., Nikooee, E., Hassanizadeh, S.M. and Grabe, J. (2018), "Theoretical and experimental investigations on the role of transient effects in the water retention behaviour of unsaturated granular soils", *Geomech. Energy Envir.*, 15, 54-64. https://doi.org/10.1016/j.gete.2018.02.003

Mualem, Y. (1974), "a conceptual model of hysteresis", *Water Resour. Res.*, **10**(3), 514-520. http://doi.org/10.1029/wr010i003p00514.

Niu, G., Shao, L., Sun, D. and Guo, X. (2020), "A simplified directly determination of soil-water retention curve from pore size distribution", *Geomech. Eng.*, **20**(5), 411-420. http://doi.org/10.12989/gae.2020.20.5.411.

O'Carroll, D.M., Phelan, T.J. and Abriola, L.M. (2005), "Exploring dynamic effects in capillary pressure in multistep outflow experiments", *Water Resour. Res*., **41**(11), W11419. http://doi.org/10.1029/2005WR004010.

Otalvaro, I.F., Neto, M.P.C., Delage, P. and Caicedo, B. (2016), "Relationship between soil structure and water retention properties in a residual compacted soil", *Eng. Geol*., **205**, 73-80. https://doi.org/10.1016/j.enggeo.2016.02.016.

Pham, H.Q., Fredlund, D.G. and Barbour, S.L. (2005), "A study of hysteresis models for soil-water characteristic curves", *Can. Geotech. J*., **42**(6), 1548-1568. http://doi.org/10.1139/t05-071.

Rafraf, S., Guellouz, L., Guiras, H. and Bouhlila, R. (2016), "A new model using dynamic contact angle to predict hysteretic soil water retention curve", *Soil Sci. Soc. Am. J*., **80**(6), 1433-1442. http://doi.org/10.2136/sssaj2016.01.0006.

Rahardjo, H., Meilani, I., Leong, E.C. and Rezaur, R.B. (2009), "Shear strength of compacted soil under infiltration condition" *Geomech. Eng.*, **1**(1), 35-52. http://doi.org/10.12989/gae.2009.1.1.035.

Rasool, A.M. and Kuwano, J. (2020), "Ffect of constant loading on unsaturated soil under water infiltration conditions", *Geomech. Eng.*, **20**(3), 221-232. http://doi.org/10.12989/gae.2020.20.3.221.

Sakaki, T., O'Carroll, D.M. and Illangasekare, T.H. (2010), "Direct quantification of dynamic effects in capillary pressure for drainage–wetting cycles", *Vadose Zone J*., **9**(2), 424-437. http://doi.org/10.2136/vzj2009.0105.

Smiles, D.E., Vachaud, G. and Vauclin, M. (1971), "A test of the uniqueness of the soil moisture characteristic during transient, nonhysteretic flow of water in a rigid soil1", *Soil Sci. Soc. Am. J.*, **35**(4), 534-539. http://doi.org/10.2136/sssaj1971.03615995003500040018x.

Topp, G.C., Klute, A. and Peters, D.B. (1967), "Comparison of water content-pressure head data obtained by equilibrium, steady-state, and unsteady-state methods", *Soil Sci. Soc. Am. J*., **31**(3), 312-314. http://doi.org/10.2136/sssaj1967.03615995003100030009x.

Viaene, P., Vereecken, H., Diels, J. and Feyen, J. (1994), "A statistical analysis of six hysteresis models for the moisture retention characteristic", *Soil Sci.*, **157**(6), 345-355. http://doi.org/10.1097/00010694-199406000-00003.

Wana-etyem, C. (1982), "Static and dynamic water content-pressure head relations of porous media", Ph.D. Dissertation, Colorado State University, Colorado.

Wei, C.F. and Dewoolkar, M.M. (2006), "Formulation of capillary hysteresis with internal state variables", *Water Resour. Res*., 42 (7), W07405. http://dx.doi.org/10.1029/2005wr004594

Wheeler, S.J., Sharma, R.S. and Buisson, M.S.R. (2003), "Coupling of hydraulic hysteresis and stress–strain behaviour in unsaturated soils", *Géotechnique*, **53**(1), 41-54. http://doi.org/10.1680/geot.53.1.41.37252.

Zhou, A. (2013), "A contact angle-dependent hysteresis model for soil–water retention behaviour", *Comput. Geotech*., **49**, 36-42. https://doi.org/10.1016/j.compgeo.2012.10.004.

Zhou, A.N., Sheng, D. and Carter, J.P. (2012), "Modelling the effect of initial density on soil-water characteristic curves", *Géotechnique*, **62**(8), 669-680. https://doi.org/10.1680/geot.10.P.120.

Zhou, C. and Ng, C.W.W. (2014), "A new and simple stress-dependent water retention model for unsaturated soil", *Comput. Geotech*., **62**, 216-222. https://doi.org/10.1016/j.compgeo.2014.07.012.

Zhuang, L., Hassanizadeh, S.M., Qin, C. and de Waal, A. (2017), "Experimental investigation of hysteretic dynamic capillarity effect in unsaturated flow", *Water Resour. Res*., **53**(11), 9078-9088. http://doi.org/10.1002/2017WR020895.

CC